LES for Street-Scale Environments and its Prospects

Zheng-Tong Xie and Ian P. Castro

School of Engineering Sciences, University of Southampton, SO17 1BJ, UK
z.xie@soton.ac.uk, i.castro@soton.ac.uk

Summary. In this paper we raise several issues, e.g. resolution, Reynolds number dependency, mesh quality and inflow boundary conditions for Large-Eddy Simulation (LES) of street scale flows, scalar dispersion and heat transfer within urban areas. Some of the issues are addressed extensively and some LES results of test cases are presented. The other issues are discussed and commented for further study. Finally we attempt to foresee prospects for the use of LES for urban environments with a computational domain size up to a few kilometers and a resolution down to one meter.

Key words: Urban canopy layer, cuboid-shape body, resolution, Reynolds number dependency, inflow condition, efficiency, point source dispersion, heat transfer

1 Introduction

There is a growing concern about the urban environment. In our previous work, we have demonstrated that LES is a promising tool for this area [10]. However, in order to establish the credibility of LES as a tool for operational/practical forecast applications, there are many issues which must be addressed, such as:

- Is there a general minimum resolution needed to produce reasonable turbulence statistics? If the answer is 'YES' for the flow, is it also applicable for scalar dispersion?
- Is LES reliable for the high Reynolds numbers typical of urban flows?
- How much does LES accuracy depend on the mesh quality in such cases?
- Efficient inflow boundary conditions (e.g. *via* appropriate generation of artificial turbulence) need to be coupled to the weather scale flow and the urban boundary layer. What errors are involved in doing this?

In this paper, we investigate the quality and reliability of LES for street-scale flows, mainly by undertaking numerical-sensitivity experiments, rather than attempting to quantify the uncertainty and error of LES as in [7].

2 Governing equations of Large-eddy simulation

To ensure a largely self-contained paper, a brief description of the governing equations is given here. More details can be found in [10], hereafter denoted by XC.

The filtered continuity and Navier-Stokes equations are written as follows,

$$\begin{aligned} &\frac{\partial u_i}{\partial x_i} = 0 \\ &\frac{\partial u_i}{\partial t} + \frac{\partial u_i u_j}{\partial x_j} = -\frac{1}{\rho}\left(\frac{\partial p}{\partial x_i} + \delta_{i1}\frac{\partial \langle P \rangle}{\partial x_1}\right) + \frac{\partial}{\partial x_j}\left(\tau_{ij} + \nu\frac{\partial u_i}{\partial x_j}\right) . \end{aligned} \tag{1}$$

The dynamical quantities, u_i, p are resolved-scale (filtered) velocity and pressure respectively and τ_{ij} is the subgrid-scale (SGS) Reynolds stress. δ_{i1} is the Kronecker-delta and ν is the kinematic viscosity. $\partial\langle P\rangle/\partial x_1$ is the driving force, a constant streamwise pressure gradient which exists only when periodic inlet-outlet boundary conditions are applied but otherwise vanishes. The Smagorinsky SGS model was used with $C_s = 0.1$. In the near-wall region, the Lilly damping function was also applied. Note that the Smagorinsky model is widely used by researchers to simulate the kind of flow of most concern to us – rough-wall flows – with considerable success [10].

The wall model is generally an important issue for LES, and is no less important than the SGS model if the computational cost is to be minimised. For cases where the fine eddies in the vicinity of the wall are important, it is recommended that $\mathscr{N}_1^+$ is of order of unity ($\mathscr{N}_1^+$ is the distance in wall units between the centroid of the first cell and the wall assuming the $\mathscr{N}$ coordinate is normal to the wall). Note, however, that for a complex geometry, where separation and attachment processes occur, it is impossible to satisfy this criteria everywhere. We argue that, unlike the situation for smooth-wall flows, it is in fact not necessary, at least for obtaining overall surface drag and the turbulent motions at the scale of the roughness elements (buildings), which turn out to be dominant (see XC).

The local wall shear stress is then obtained from the laminar stress-strain relationships:

$$u^+ = \frac{u}{\hat{u}_\tau}, \quad \mathscr{N}^+ = \frac{\rho\hat{u}_\tau\mathscr{N}}{\mu}, \quad \mathscr{N}^+ = u^+ , \tag{2}$$

where $\rho\hat{u}_\tau^2$ is the local wall shear stress. However, if the near-wall mesh is not fine enough to resolve the viscous sublayer, for simplicity it is assumed that the centroid of the cell next to the wall falls within the logarithmic region of the boundary layer:

$$\frac{u}{\hat{u}_\tau} = \frac{1}{\kappa}\ln E\left(\frac{\rho\hat{u}_\tau\mathscr{N}}{\mu}\right), \tag{3}$$

where κ is the von Karman constant and E is an empirical constant. The log-law is employed when $\mathscr{N}^+ > 11.2$. Again, note that for very rough-wall flows there are probably very few regions on the surface of the roughness elements where log-law conditions genuinely occur in practice; however, we have shown earlier that for this type of flow the precise surface condition is unimportant for capturing the element-scale flows and surface drag (see XC).

The entire LES model was implemented in the code described in XC. Crucially, the discretisation for all terms in Eq. (1) was second order accurate in both space and time – lower-order schemes were found not to be adequate but, equally, for the kind of problems addressed here it is not necessary to use schemes that are of even higher order. Inlet boundary conditions were set using a User-Defined-Function, embodying the technique described in the following section.

3 Reynolds number dependency and minimum resolution

Recently an LES model was used to calculate the turbulent flow over staggered wall-mounted cubes and a staggered array of random height obstacles with area coverage 25%, at Reynolds numbers between 5×10^3 and 5×10^6, based on the free stream velocity and the obstacle height [10]. Three meshes with $8 \times 8 \times 8$, $16 \times 16 \times 16$ and $32 \times 32 \times 32$ grid points respectively per building block were used for flow at the various Reynolds numbers. The significantly coarser mesh than required for a full DNS, i.e. $16 \times 16 \times 16$ grid points per building block, produces sufficiently accurate results. Turbulence generated by urban-like obstacles, e.g. cuboid-shape bodies with sharp edges, is building-block-scale dominated, which suggests that for this type of flow the precise wall condition/subgrid-scale model is unimportant for capturing the element-scale flows and surface drag.

$Re = 5 \times 10^3$ is low enough for the $32 \times 32 \times 32$ resolution to be 'almost' DNS, but flows at $Re = 5 \times 10^4$ and $Re = 5 \times 10^6$, with coarse or fine grids, generated almost identical non-dimensional statistics compared with those at $Re = 5 \times 10^3$, even though the high-frequency end of the spectrum was not well captured in some cases. Also, surface drag obtained using the same resolution was comparable between various Reynolds numbers, as also found in laboratory experiments. The results collectively confirm that Reynolds number dependency, if it does exist, is very weak (except no doubt very close to solid walls), principally because the surface drag is predominantly form drag and the turbulence production process is at scales comparable to the roughness element sizes, as suggested also by wind tunnel experiments.

LES is thus able to simulate turbulent flow over the urban-like obstacles at high Re with grids that would be far too coarse for adequate computation of corresponding smooth-wall flows. A wide inertial sub-range in flows over urban-like obstacles may also suggest that turbulence reaches a quasi-isotropic state at relatively lower frequency than non-vortex-shedding flows at similar

Reynolds numbers, which is another reason why a simple SGS model can give reasonable results. Whilst improvement of the SGS model, *via* more expensive dynamic models for example, may enhance the simulation in the close vicinity of the solid walls at high Reynolds number and, likewise, improvements in the wall model itself may increase accuracy near the element walls, it is much more important to use grids which can resolve the major features of the separated shear layers. The influence of the small-scale motions, captured increasingly inadequately as Re rises, is much lower in these flows than it is in smooth-wall equivalents. This is all greatly beneficial for the numerical simulation of the coupling between weather scale flows and street scale flows. Our major conclusion is thus that LES may be reliably able to simulate turbulent flow over urban areas at realistic Reynolds numbers, with what (in more 'classical' flows) would normally be thought of as inadequate grids. It is suggested that medium sized meshes on the body scale (e.g. 15-20 grid points at least over a typical body dimension) are sufficient for the simulation of a real urban area, at least for obtaining the total drag force or the large-scale flow dynamics.

4 Mesh type and wall-layer resolution

4.1 Tetrahedral mesh vs. hexahedral mesh

In the computations discussed above, only Cartesian (hexahedral) meshes were used for generic surfaces. In order to simulate the flows over a genuine urban canopy with a more complex geometry, unstructured non-hexahedra meshes inevitably have to be used. Tetrahedral meshes are widely used in CFD because methods which do this are mature, efficient and highly automated [8]. It is worth investigating the reliability and accuracy of the tetrahedral mesh for LES of the urban-type flows.

Fine and coarse tetrahedral meshes (see Fig.1) were used to simulate the flows in the same computational domain ($4h \times 4h \times 4h$; h cube height) as in [10] for an array of uniform staggered cubes, i.e. four cubes with area coverage 25%. The lengths of the side of the tetrahedral cells were approximately $h/16$ and $h/8$ respectively for fine and coarse meshes(1.3M cells and 0.16M cells respectively in total). The Reynolds number was 5×10^3 based on the free stream velocity and the cube height. The other settings were the same as those in [10].

Fig.2 shows a typical comparison of vertical profiles of the turbulence statistics behind a cube using the hexahedral mesh ($16 \times 16 \times 16$ grid points per cube) and the tetrahedral meshes. Clearly, increasing the resolution of the tetrahedral mesh improves the profiles. However, even the fine tetrahedral mesh (1.3M cells) evidently underestimates the turbulence fluctuations compared to the hexahedral mesh (0.25M cells). Perhaps not surprisingly, the accuracy of the tetrahedral meshes, even at the higher resolution, is confirmed as being not so high as that of the uniform hexahedra mesh.

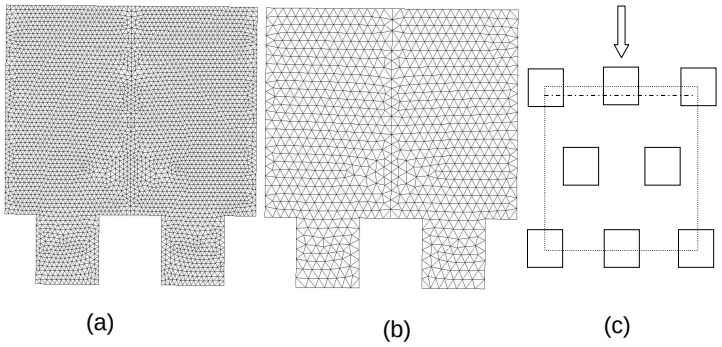

Fig. 1. A vertical cut on the chain-dotted line in (c) of tetrahedral meshes for an array of uniform cubes. (a), fine mesh(1.3M cells); (b), coarse mesh(0.16M cells); (c), the square highlighted by the dotted line indicates the plan view of the computational domain.

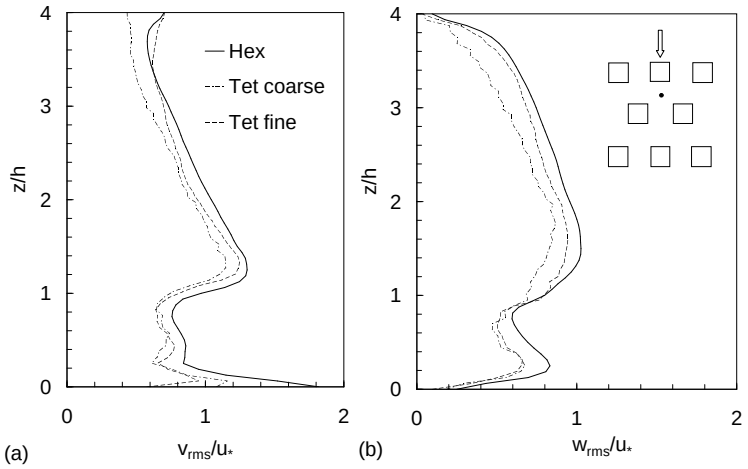

Fig. 2. Comparison of vertical profiles of the turbulence statistics behind cube (indicated by the dot in the inset in (b) using hexahedral (0.25M cells) and tetrahedral meshes. (a) spanwise and (b) vertical fluctuation velocities.

4.2 Polyhedral mesh vs. hexahedral mesh

Polyhedral meshes offer substantially better properties than tetrahedral meshes [8]. However, there is relatively little experience available with such meshes. A polyhedral mesh was validated for flow over (initially) uniform cubes and then a more random geometry (i.e. 64 staggered blocks with random heights). Only the latter is reported here.

The size of a 'repeating unit' of the obstacle array was 80 mm × 80 mm, within which were placed in regular staggered pattern sixteen 10-mm-square elements having heights chosen from an appropriate normal distribution. Four repeating units were included in the whole computing domain (hence the total number of obstacles is 64), so the domain size was $L_x \times L_y \times L_z = 16h_m \times 16h_m \times 10h_m$, where $h_m = 0.01$m is the mean height of the obstacles. The Reynolds number was 5000 based on the free stream velocity and the mean height. A three-level hexahedral mesh (2.3 million cells) with $16 \times 16 \times 16$ cells per $h_m \times h_m \times h_m$ in the near wall region (see Fig. 3c), and a three-level polyhedral mesh (1.3 million cells) with $13 \times 13 \times 13$ cells per $h_m \times h_m \times h_m$ in the near wall region (see Fig. 3d) were used.

Essentially identical results were obtained using the polyhedral mesh and hexahedral mesh, despite the much smaller number of cells used in the former. This may suggest that the two meshes are both satisfactory. It is known that the former is more flexible for complex geometry than the latter. Furthermore, the results confirm that the polyhedral mesh is more accurate and less memory

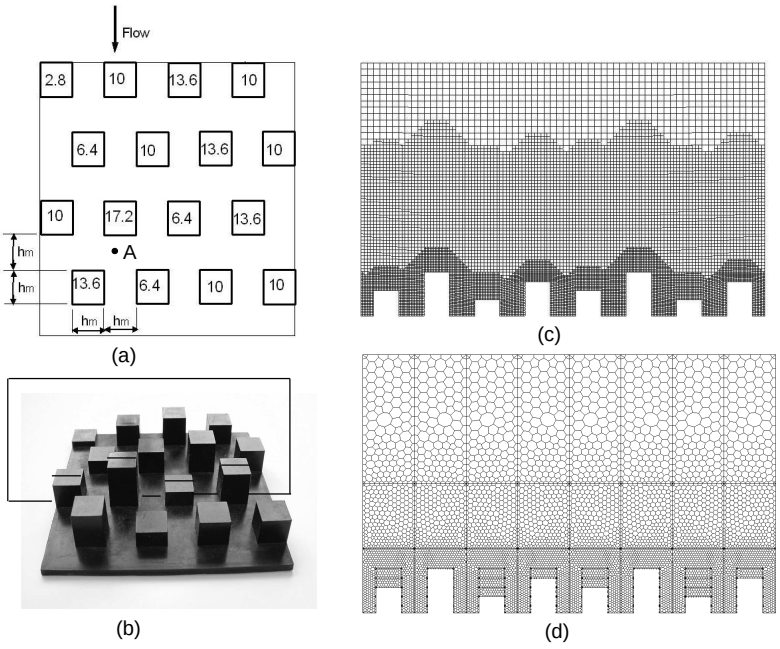

Fig. 3. (a), plan view of one repeating unit with numbers indicating the block height in mm; (b), a view of one repeating unit used in the laboratory experiment [3]; (c), hexahedral mesh ($16 \times 16 \times 16$ grids on the 10mm cube, 2.3M cells); (d), polyhedral mesh ($13 \times 13 \times 13$ grids on the 10mm cube, 1.3M cells), for an array of obstacles with random heights.

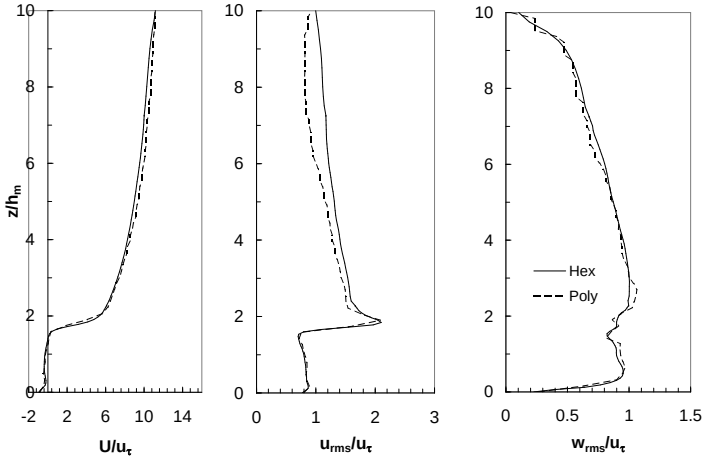

Fig. 4. Vertical profiles of mean velocity and turbulence statistics behind 17.2mm block (i.e. station A in Fig.3a) using hexahedral and polyhedral meshes.

consuming than the widely used tetrahedral mesh. Fig. 4 presents streamwise mean velocity and velocity r.m.s profiles behind the 17.2 mm block, i.e. station A in Fig. 4a.

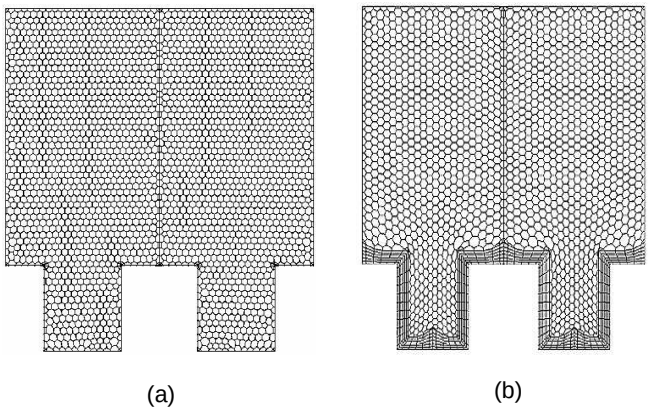

Fig. 5. Polyhedral meshes without (a) and with (b) wall-layers for an array of uniform cubes. Computational domain as in Fig.1c.

4.3 Importance of wall-layer resolution

How important are the wall-layers on the building surfaces? The computation domain typically may contain tens or hundreds of buildings. For instance,

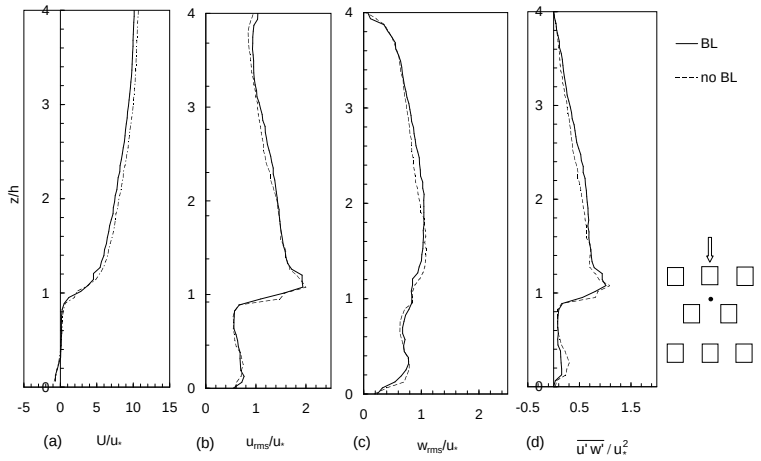

Fig. 6. Comparison of vertical profiles of mean velocity and turbulence statistics between meshes with (BL, C20SB) and without (no BL, C20SA) wall-layers.

the DAPPLE geometry (http://www.dapple.org.uk/), which is one we are currently simulating, has nearly one hundred buildings. To resolve all of the wall layers would be extremely expensive at present.

LES was applied to calculate the turbulent flow over staggered wall-mounted uniform cubes with area coverage 25% at Reynolds number of 5000 based on the free stream velocity and the cube height. The computational domain and the other settings were the same as those in §4.1. A pure polyhedral mesh of more than 0.1 million cells with $13 \times 13 \times 13$ grid points per cube was used (Fig. 5a, C20SA). A second polyhedral mesh with a similar number of cells but with five wall-layers on the solid surfaces was also used (Fig. 5b, C20SB). The distances in wall units of the centroid of the first cell from the wall, z_1^+, for C20SA and C20SB were approximately 7.8 and 1 respectively, based on the global friction velocity u_*. Note that the distances in wall units of the centroid of the first cell from the wall based on the local friction velocity, z_{l1}^+, were much lower, because obstacle form drag provides the dominant part of the total drag. Fig. 6 shows a comparison of vertical profiles of normalised mean streamwise velocity U, velocity fluctuations u_{rms} & w_{rms} and Reynolds shear stress $-\overline{u'w'}$. The differences between "BL" and "no BL" are hardly discernible, which suggests that it is not crucial to resolve the wall-layers on the building surfaces if the details within the wall-layers are not of particular interest.

By using numerical experiments like these, we have concluded that full resolution of the wall-layers is not important for the global turbulence statistics, nor for the mean drag of the complete surface. Note, however, that if heat transfer processes are important the same conclusion may well not hold.

5 Inflow conditions and large-scale unsteady flows

Coupling weather-scale computations (for example from the UK Met Office's weather code, the Unified Model) to smaller-scale computations of flow and dispersion within urban environments requires a particularly efficient means of providing dynamically changing turbulence data at the inlet of the computational domain. This is especially true if the street-scale flows are to be modelled using LES.

Autocorrelation functions of typical turbulent shear flows have forms not too dissimilar to decaying exponentials. A digital-filter-based generation of turbulent inflow conditions exploiting this fact was developed [11] as a suitable technique for LES computation of spatially developing flows. The artificially generated turbulent inflows satisfy prescribed profiles of integral length scales and the Reynolds-stress-tensor. The method is more suitable for developed turbulent shear flows, e.g. the flow over an urban area, than the one proposed by [6]. It is also much more efficient than, amongst others, Klein's methods because at every time step only one set of two-dimensional (rather than three-dimensional) random data is filtered to generate a set of two-dimensional data with the appropriate spatial correlations. These data are correlated with the data from the previous time step by using an exponential function based on two weight factors.

In [12], LES of plane channel flows and flows over a group of staggered cubes has provided satisfactory validation of the technique, with results showing good agreement with simulations using periodic inlet-outlet boundary conditions and reasonable agreement with data from other sources – both DNS and laboratory experiments. These satisfactory validations, the fact that the results are not too sensitive to the precise form of the prescribed inlet turbulence, and the high efficiency of the technique, together suggest that the method will be very useful for practical simulations of urban-type flows.

Understanding the mechanism by which the urban boundary layer and the regional weather model are coupled aerodynamically and thermodynamically is known to be vital but is still in its infancy. Unsteadiness of the large scale driving wind probably has significant impact on the turbulent flows within the urban boundary layer [9]. For implementing dynamic spatial boundary conditions derived from the unsteady output of much larger-scale computations, like those available from the UK Met Office's Unified Model (UM), coupled with the new small-scale turbulence inflow method described as in §5, tools need to be developed to simulate flows over genuine urban geometry.

The question arises as to how such tools can be validated. Both pure oscillatory flow and a combined oscillatory flow with an added mean current have attracted researchers' attention for decades, with most studies being experimental [1, 2, 9]. As a validation, for investigating unsteady large-scale driving flows, we numerically simulated a combined oscillatory throughflow and mean current (here labelled as C20SOI) over a group of cube arrays (eight rows of cubes, see Fig. 9c) using the inflow-generating method. An assumption was

made here that at the inlet the turbulent fluctuations ($u_{rms}, v_{rms} and w_{rms}$) are in phase with the mean streamwise velocity defined by

$$U = U_0[1.0 + 0.5\sin(2\pi t/T)], \tag{4}$$

where U is the phase averaged streamwise velocity, U_0 is the mean streamwise velocity of the current, $T = 322.6h/u_*$ is the (relatively long) oscillation period, h is the height of the cube and u_* is the mean friction velocity. This assumption might not be too unreasonable for street-scale urban flows which are driven by the geostrophic wind.

For the same computational domain, a second LES run was conducted with a combination of a steady and an oscillatory pressure gradient and with streamwise periodic boundary conditions. This is labelled C20SOP and the unsteady pressure gradient is defined by

$$\frac{dP}{dx} = -\frac{\rho}{D}\{u_*[1.0 + 0.5\sin(2\pi t/T)]\}^2, \tag{5}$$

where $D = 4h$ is the depth of the domain and ρ is the density. The resulting mean streamwise velocity can be written as $U = U_0[1 + \alpha\sin(2\pi t/T - \phi)]$, where α and ϕ (the phase lag) are parameters to be obtained by using a fitting method. The velocity $r.m.s$ values ($u_{rms}, v_{rms}, w_{rms}$) are assumed to be of similar form to this equation.

Results obtained from the two driving methods are illustrated in Fig. 7, which shows the algebraically averaged profiles of the phase-averaged statistics obtained by the two methods and compared with the previous steady flow case (§4.1). The 'Oscillatory, body force' case is in marginally better agreement with the 'Steady, body force' than the 'Oscillatory, inflow' case, in particular within the canopy. The discrepancies might have two sources: (1) in Eq.5 there is a higher frequency component, $\rho\{u_*0.125[1 - \cos(4\pi t/T)]\}$; (2) the phase of U, $u_{rms}, v_{rms}, w_{rms}$ lags that of dP/dx (see Eq. 5).

Hence, an investigation of the mechanisms in the combined oscillatory throughflow superposed on a mean current was also attempted. We found that the phase lags of U, $\overline{u'w'}$, u_{rms} and w_{rms} are approximately 45 degree at all heights for C20SOP. This is reflected in the surface drag; Fig. 8 shows time series of the driving force, i.e. the body force in Eq.5, and the total instantaneous drag on the sixteen cubes; a clear 45 degree phase lag is seen.

Fig. 9 shows a comparison of phase averaged streamwise velocity between C20SOI and C20SOP. Note that here for C20SOP the phase is $2\pi t/T - \phi$ and that the phase-averaged statistics for C20SOI were obtained behind row seven (the 'dot' in fig.7, r.h.s.). Fig. 9b shows that at all heights for C20SOI the streamwise velocity keeps the same phase, whereas Fig. 9a for C20SOP shows a very slight variation of phase lag with height. Nevertheless, the data in Fig. 9a and b have an almost identical pattern. The phase averaged turbulence statistics (u_{rms}, w_{rms} and $\overline{u'w'}$) also show almost identical patterns in the two cases. We conclude that our inflow turbulence generation method is adequate for cases where there are long-time-scale variations at the upstream boundary.

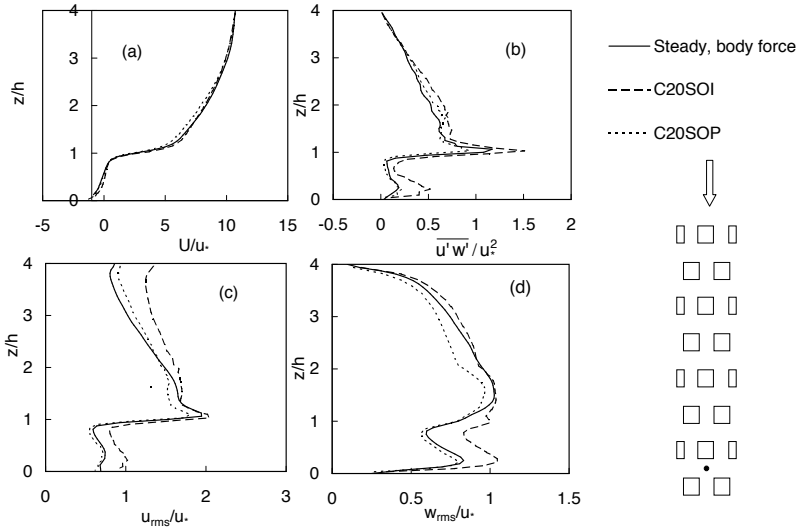

Fig. 7. Algebraically averaged profiles of the phase-averaged statistics.

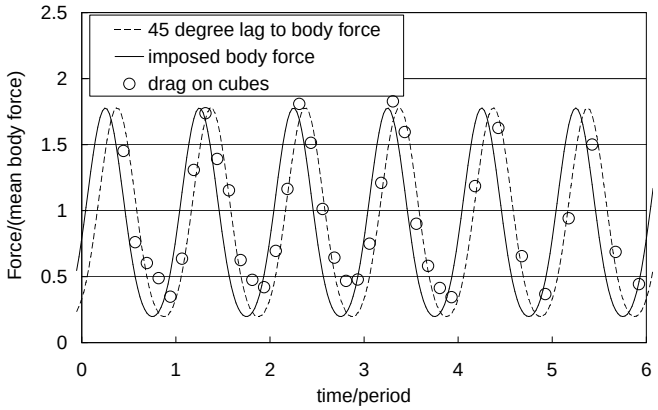

Fig. 8. Driving force and total instantaneous drag on cubes.

6 Conclusions

Currently such LES simulations (using steady large-scale boundary conditions obtained from the UM), like those for the Marylebone Road area of London recently studied at both field and laboratory scale under the DAPPLE project (http://www.dapple.org.uk/), are showing great promise. The inflow and polyhedral mesh techniques have been applied for the turbulent flow and point source dispersion over the DAPPLE field site, which is located at the intersection of Marylebone Road and Gloucester Place in Central London. The computational domain size was 1200m (streamwise) x 800m (lateral)

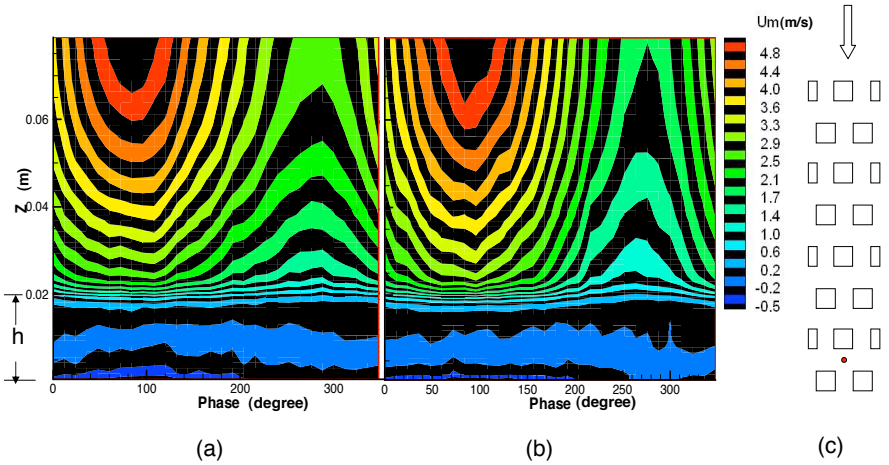

Fig. 9. Vertical profiles of phase averaged streamwise velocity. (a), C20SOP: body force driving; (b), C20SOI: inflow; (c): plan view of the 8 rows of cubes.

x 200m (in full scale), with a resolution down to approximately one meter. Numerical simulations have focused on the case of southwesterly winds and a tracer release at York St. between Monatgue St. and Gloucester Place. The mean velocity and the Reynolds stress profiles at fourteen sites and mean concentration at ten sites are in good agreement with the wind tunnel experiments conducted under the DAPPLE programme (at EnFlo, University of Surrey) and, incidentally, have been found to be significantly better than results obtained using RANS techniques.

On the basis of our current success, we are optimistic about the reliability and affordability of LES for simulating flow and scalar dispersion within and above usefully-sized sub-domains of a city region, at a resolution down to one meter. Problems involving significant heat transfer effects are, however, likely to pose even greater challenges.

Acknowledgement. The support of the Natural Environment Research Council under NCAS Grant DST/26/39 is gratefully acknowledged.

References

1. Al-Asmi K (1992) *PhD Thesis, Depart. Mech. Eng., University of Surrey.*
2. Chang YS and Scotti A (2004)*J. Geohys. Res.* 109:1-16.
3. Cheng H. and Castro I.P. (2002) *Boundary-Layer Meteorol.* 104: 229-259.
4. Lim HC, Castro IP & Hoxey RP (2007) *J. Fluid Mech.* 571:97-118.
5. Lodahl CR, Sumer BM and Fredsøe J. (1998) *J. Fluid Mech.* 373:313-348.
6. Klein M, Sadiki A and Janicka J (2003) *J. Comp. Phys.*, 86:652-665.
7. Roache PJ (1997) *Annu. Rev. Fluid Mech.* 29:123-160.
8. Peric M (2004) ERCOFTAC bulletin 62:25-29.
9. Sleath JFA (1987) *J. Fluid Mech.* 182:369-409.
10. Xie Z-T & Castro IP (2006) *Flow, Turbulence and Combustion*, 76(3): 291-312.
11. Xie Z-T & Castro IP (2006) *J. Hydrodynamics, Ser. B*, 18(3, Sup.1): 259-264.
12. Xie Z-T & Castro IP (2007) *Flow, Turbulence and Combustion*, submitted.